Key Engineering Materials Vol. 633 (2015) pp 93-97
© (2015) Trans Tech Publications, Switzerland
doi:10.4028/www.scientific.net/KEM.633.93

Submitted: 04.06.2014
Accepted: 17.06.2014

Densification Behavior and Microstructure Evolution of LTCC Film Constrained by Rigid Substrate

Shishun Qi, Ruzhong Zuo* and Zhaosheng Ma

Institute of Electro Ceramics & Devices, School of Materials Science and Engineering, Hefei University of Technology, Hefei 230009, China

piezolab@hfut.edu.cn (Corresponding Author)

Key Words: Sintering, LTCC, Constrained Film, Anisotropy

Abstract. LTCC films constrained by rigid substrate were sintered at different temperatures ranging from 760 °C to 800 °C. An optical dilatometer together with a rocking arm was employed to record sintering strains of the constrained films during the sintering process. The densification behavior of constrained films was systematically studied through the measured sintering strains by comparing with that of freely sintered films. For the constrained films, the final density was smaller and the activation energy for the densification was larger than that of the freely sintered ones. Moreover, anisotropic microstructure was induced by the tensile stress.

Introduction

Low-temperature co-fired ceramics (LTCC), which enable the integration of various passive components, exhibit great potential in several application areas like wireless communication, sensor technology, electronic control units and micro-systems [1]. During the cofiring process, cambers, flaws and cracks across would occur, which are major concerns for the fabrication of large, flat multilayer ceramic modules [2]. Constrained sintering has been widely developed and a variety of methods have been applied to cope with the stringent requirements of dimensional accuracy [3]. As a model of constrained sintering, film constrained by rigid substrate is not only a typical feature of many ceramic processing technologies, but also a topic of considerable fundamental interest [4]. In the case, the film is fully constrained by the in-plane tensile stress and shrinkage takes place only in the thickness direction [3]. To gain deep understanding of the constrained sintering process, an isotropic formulation based on a continuum mechanic model has been extensively applied [4-7]. Nevertheless, Garino and Bowen have found that the data predicted by the model is able to fit the experimental data for glass films, but not for the polycrystalline ZnO and Al_2O_3 [4]. Guillon et al. has also carried out investigations on alumina films and concluded that anisotropic microstructure develops as the sintering proceeds [8]. However, to the best of our knowledge, there has been no detailed research on the densification process of LTCC films constrained by rigid substrates.

In present paper, LTCC constrained films were prepared through tape-casting. An optical dilatometer together with a mechanically amplified system was designed to record the sintering strains. Studies on the sintering kinetics and the microstructure were also conducted.

Experimental

LTCC films were deposited on alumina substrates through a typical tape casting method by using commercial ceramic powder (ε=8.5, Infine Neo-Material Co., Ltd, Yunnan, China). The reference axes for the film are: x for the tape casting direction, y the transverse and z the thickness direction. An optical dilatometer has been designed to record the sintering strains during the sintering process [9]. And a quartz rocking arm was used as a mechanical amplified system to facilitate the record of sintering strains. The schematic of the quartz rocking arm could be seen in Fig. 1. Owing to the specific geometry, negligible load was applied on the film surface. The distance between the bottom holder and the rocking arm was measured by our optical dilatometer. The thermal expansion of the

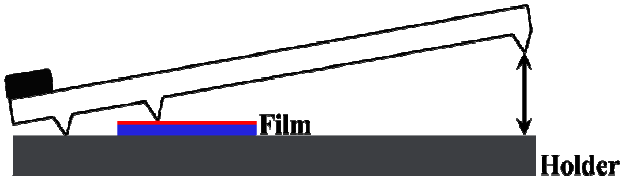

Fig. 1 Schematic of the system to measure the shrinkage of the constrained film

system was deducted when calculating the strain. For the free sintering case, ten layers of cast films were alternatively laminated to facilitate the measurement of the sintering strains. And the sintering strain in the x-y direction was used as the free sintering strain. Two specimens were tested for each temperature, and the mean value of strain was utilized for further calculation. Validation of the measured strain was performed by comparing the strain measured through the scanning electron microscopy and a good agreement was achieved.

To characterize the microstructure of the investigated free and constrained films, films with the same density were used. The sintered films were fractured in the y-z plane. Each specimen was carefully ground and polished to a 5 μm finish. The polished surfaces were then coated with a thin gold conductive layer for the examination of the pore morphology by a scanning electron microscope (SEM, SSX-550, Shimadzu, Japan). The length and angle of pores in the SEM image were determined through the image software (Adobe Photoshop CS6). Then, the pore orientation was obtained by analyzing the statistical data acquired from the images.

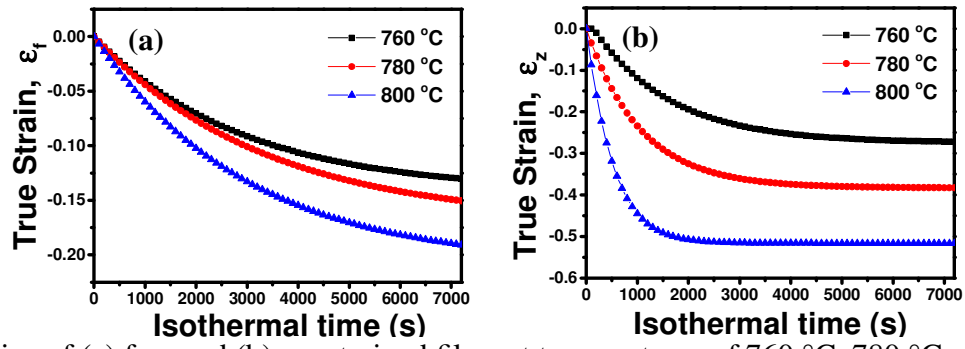

Fig.2 Strains of (a) free and (b) constrained films at temperatures of 760 °C, 780 °C and 800 °C as a function of isothermal time

Results and Discussion

The sintering schedule was well determined to guarantee the complete binder burnout without film cracking. Free and constrained films were sintered at temperatures of 760 °C, 780 °C and 800°C. Fig. 2 provides the strain measured for freely and constrained sintered films as a function of isothermal time. The true strain definition was used, rather than engineering strains in the calculation of sintering strains because of the large deformation involved in sintering. By assuming isotropic shrinkage for the freely sintered film, the strains were determined through the in-plane (x-y) dimension changes. However, shrinkage was only occurred in the thickness direction (z) for the constrained films. As shown in Fig. 2(a), the free strain ε_f increased with the isothermal time and larger strain could be seen at higher sintering temperature. Fig. 2(b) displays the strain in the thickness direction ε_x for the constrained films, which was found to be much larger than ε_f in freely sintered films. And it could be attributed to the fact that all the densification took place along the thickness direction in the constrained films.

As sintering proceeded, the density could be computed from the obtained strains. Equation (1) was used for the density computation in free sintering case. During constrained sintering, the film shrunk only in the thickness direction ($\varepsilon_x = \varepsilon_y = 0$) and the equation (2) was used:

$$\rho=\rho_0 \exp(-3\varepsilon_f) \quad (1)$$

$$\rho = \rho_0 \exp(-\varepsilon_z) \tag{2}$$

where ρ_0 was the film density at the beginning of isothermal time. ε_f and ε_x were the strains for the freely and constrained sintered films. The calculated densities for the freely and constrained sintered films as a function of isothermal time are shown in Fig. 3(a) and Fig. 3(b). It could be seen from Fig. 3(a) that the density increased continuously as the isothermal time increased. The final relative density for the freely sintered film could reach 70%, 80% and 90% for sintering temperatures 760 °C, 780 °C and 800°C, respectively. In contrast, only 56%, 70% and 80% were obtained for the constrained films as shown in Fig. 3(b). Moreover, the density of the constrained film reached a plateau value after 2000s, as most densification has already taken place in the early isothermal stage. It could be seen that the final density for the constrained sintered film was lower than that of the freely sintered sample.

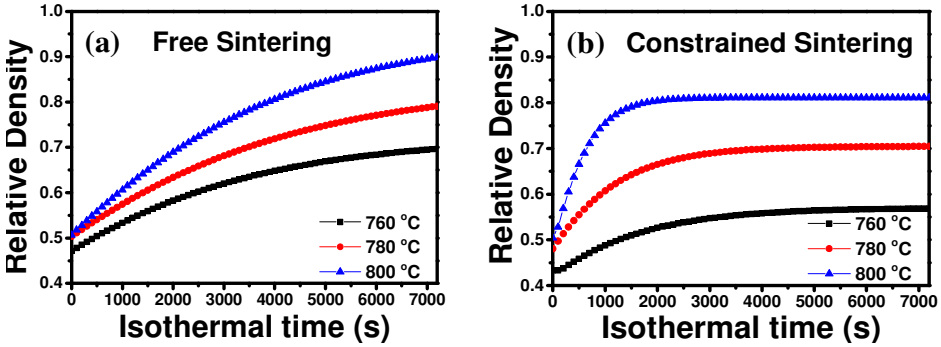

Fig.3 Density of (a) free and (b) constrained films as a function of isothermal time

The observed difference in the final density was closely related with the sintering kinetics. To obtain a better understanding of the problem, the activation energies for densification in the two types of films were calculated. The densification rate could be related to the activation energy by the equation (3) [2, 6]:

$$\dot{\rho} = \frac{k}{T} \bullet \exp(-\frac{Q}{RT}) \bullet f(\rho) \tag{3}$$

where k is a coefficient related to the grain size and surface energy, T is the absolute temperature, Q is the activation energy and R is the gas constant. According to the above equation, the activation energy Q could be determined by plotting (ρ*T) vs (1/T) at a given relative density. As a large discrepancy could be observed in the early isothermal stage, a relative low density of 55% was used in the calculation and the results for the free and constrained films were shown in Fig. 4. The slopes for the densification rate profiles were extracted as the activation energy for the densification process. And the activation energies were obtained as 20 ± 1.4 kJ/mol and 102 ± 19.5 kJ/mol for the freely and constrained film, respectively. Larger activation energy for the constrained film was also reported by Lin and Choe [2, 6]. The larger activation energy in the constrained film could be mainly attributed to the in-plane tensile stress.

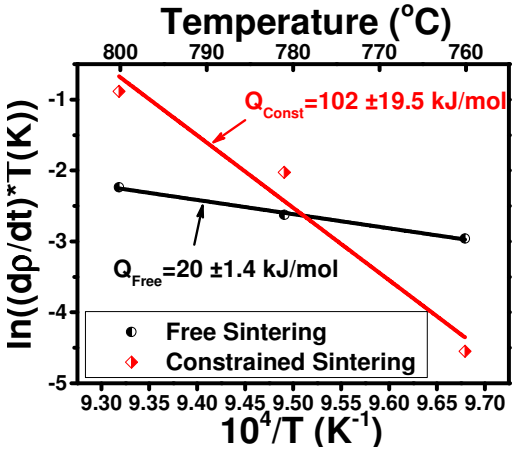

Fig.4 Plot of ln(ρ*T) vs (1/T) at relative density of 55% for free and constrained films

Moreover, the external applied stress would also lead to anisotropic microstructure and pore orientation was usually used to evaluate anisotropy [10]. Due to the complexity of pore geometries, the long axis of each pore together with its corresponding angle to the y direction was used to describe the pore orientation. A

series of SEM images of the cross section containing three hundred of pores were taken. The quantitative analysis for the pore orientation was conducted by cumulating pore length lying in a defined angle range and the results were normalized with the maximal value.

The obtained polar plots for the free and constrained film sintered at 800 °C at a relative density of 80% are shown in Fig. 5. For the freely sintered film, a SEM image was shown in Fig. 5(a) and the pore orientation appears completely random, which could be seen from Fig. 5(c). By comparison, pores in the constrained film exhibited preferred orientation parallel to the substrate, which could be seen from Fig. 5(b) and Fig. 5(d). Usually, anisotropy is closely related with the densifying mechanism and external stress. The LTCC film studied here is a densified based on viscous flow. Due to the biaxial tensile stress from the substrate, the viscous flow would more likely to transfer along the substrate direction, which would lead to elongated pores aligning parallel to the substrate as densification proceeded. Therefore, anisotropic microstructure would form for constrained films during the sintering process.

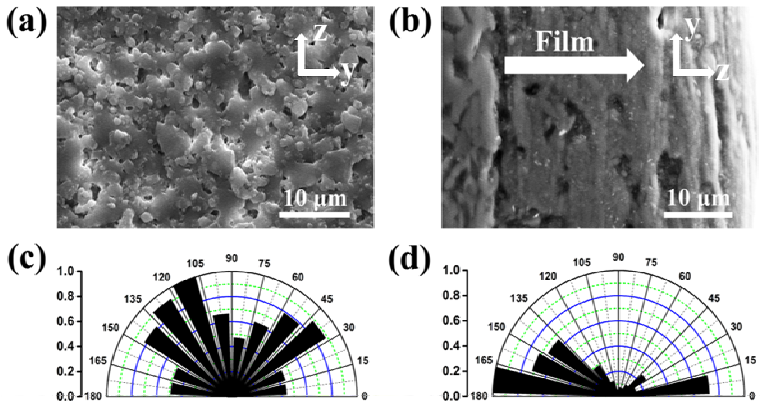

Fig.5 SEM images for the cross section of the (a) freely and (b) constrained sintered films with a density of 80% and qualitative analysis of the pore orientation for (c) free and (b) constrained films

Summary

LTCC films constrained by rigid substrate were sintered at different temperatures ranging from 760 °C to 800 °C and the densification behavior was studied by using the sintering strains measured through an optical dilatometer together with a rocking arm. It was found that the final density for the constrained film was smaller than that of free films. The activation energy for densification was found to be much larger in the constrained film, which could be attributed to the in-plane tensile stress. Moreover, anisotropy was induced by the in-plane tensile stress during the constrained sintering process and pores were more prone to aligned parallel to the substrate.

Acknowledgement

This work was financially supported by the National Natural Science Foundation of China (51272060).

References

[1] A. Mohanram, G. L. Messing, D. J. Green, J. Am. Ceram. Soc. 88 (2005) 2681-2689.

[2] Y. C. Lin, J. H. Jean, J. Am. Ceram. Soc. 87 (2004) 187-191.

[3] A. Mohanram, S. H. Lee, G. L. Messing, J. Am. Ceram. Soc. 89 (2006) 1923-1929.

[4] D. J. Green, O. Guillon, J. Rödel, J. Eur. Ceram. Soc. 28 (2008) 1451-1466.

[5] T. J. Garino, H. K. Bowen, J. Am. Ceram. Soc. 73 (1990) 251-257.

[6] J. W. Choe, J. N. Calat, G. Q. Lu, J. Mater. Res. 10 (1995) 986-994.

[7] R. K. Bordia, G. W. Scherer, Acta Metall. 36 (1988) 2393-2397.

[8] O. Guillon, S. Krauß, J. Rödel, J. Eur. Ceram. Soc. 27 (2007) 2623-2627.

[9] L. P. Yu, S. S. Qi, R. Z. Zuo, Ceram. Int. 40 (2014) 9367-9375.

[10] R. Z. Zuo, E. Aulbach, R. K. Bordia, J. Am. Ceram. Soc. 86 (2003) 1099-1105.